JOURNAL OF GEOPHYSICAL RESEARCH, VOL. 103, NO. C2, PAGES 3217–3232, FEBRUARY 15, 1998

Vertical profiles of longshore currents and related bed shear stress and bottom roughness

A. F. Garcez Faria,[1] E. B. Thornton, T. P. Stanton, C. V. Soares,[2] and T. C. Lippmann[3]

Naval Postgraduate School, Monterey, California

Abstract. The vertical structure of the mean wave-driven longshore current over a barred beach is examined on three strong current days during the DUCK94 experiment, and it is found that the bottom boundary layer is well described by a logarithmic profile (mean correlation coefficient for all 22 profiles, 0.98). The logarithmic profile fits better in the trough, where turbulent bottom boundary layer processes predominate, than over the bar, where breaking-wave-induced turbulence generated at the surface modifies the profile. The surface layer in the presence of waves is well described by adjusting the logarithmic profile for the intermittent presence of water and adding the alongshore component of the mass transport velocity (slope of the least squares linear regression between model predictions and observations, 1.005 and root-mean-square (rms) error of 7%). Bed shear stresses calculated from logarithmic velocity profiles are equated to a quadratic bottom shear stress formulation. The associated bed shear stress coefficients vary by more than an order of magnitude across the surf zone (0.0006–0.012). Bottom roughness was measured throughout the nearshore using a sonic altimeter mounted on a moving platform. The bed shear stress coefficients are positively correlated with bottom roughness (linear correlation coefficient, 0.6). A higher linear correlation coefficient (0.8) is obtained by subtracting skin friction from the total bed shear stress.

1. Introduction

Knowledge of the bottom boundary and surface layers is fundamental to understanding nearshore hydrodynamics and sediment processes. For steady flow, such as in a river, the bottom boundary layer is well described by a logarithmic profile. Only limited wave-driven, longshore current vertical profiles have been measured. *Visser* [1986] measured wave-driven longshore currents in a laboratory experiment using micropropeller and laser Doppler velocimeters and found profiles approached a logarithmic form. In a similar laboratory wave-driven longshore current experiment using laser velocimeters, *Simons et al.* [1992] verified that the vertical profiles tended to be logarithmic.

The velocity profile of a steady current is modified by the presence of waves. The superposition of waves on the mean current produces enhanced bottom friction [e.g., *Grant and Madsen*, 1979; *Christoffersen and Jonsson*, 1985; *Myrhaug and Slaattelid*, 1989; *Sleath*, 1990]. As a result, the vertical gradient of the mean current near the bed is increased, and a more uniform profile can be expected throughout most of the water column. The influence of waves is inversely proportional to water depth and wave frequency, with decreasing importance of nonlinear interactions between waves and currents within the wave-bottom boundary layer with increasing depth and frequency.

Turbulence induced by breaking waves modifies the vertical profile of longshore currents. The downward momentum mixing produced from wave breaking-injected turbulence results in a more uniform velocity profile. *Fredsoe and Deigaard* [1992] and *Church and Thornton* [1993] argue that this would result in an increased bed shear stress.

In the following, mean longshore current profiles obtained over a barred beach are examined with the objectives of (1) testing the hypothesis that the turbulent bottom boundary layer of the mean longshore current is logarithmic, (2) investigating the influence of the surface layer on the mean longshore current profile, and (3) examining the relationship between bottom shear stress and bottom roughness, including the influence of ripples and megaripples.

2. Theory

The vertical profile of longshore currents is significantly affected by the bottom boundary and surface layers. The bottom boundary layer assumes more importance since it determines the general logarithmic profile shape over most of the water column. However, processes in the surface layer can modify the profile in the presence of waves and wind.

2.1. Bottom Boundary Layer

Neglecting molecular viscous stresses, the alongshore momentum equation (y direction) is written

$$\frac{\partial \rho v}{\partial t} + \frac{\partial \rho v u}{\partial x} + \frac{\partial \rho v^2}{\partial y} + \frac{\partial \rho w v}{\partial z} = -\frac{\partial p}{\partial y} \qquad (1)$$

The velocities are expanded into mean, turbulent, and wave-induced components, $u_i = U_i + \acute{u}_i + \tilde{u}_i$ and $w = \acute{w} + \tilde{w}$,

[1]Now at Marinha-Diretoria de Hidrografia e Navegação, Rio de Janeiro, Brazil.

[2]Now at Marinha-Instituto Hidrográfico, Lisbon, Portugal.

[3]Now at the Scripps Institution of Oceanography, La Jolla, California.

Paper number 97JC02265.
0148-0227/98/97JC-02265$09.00

where ($i = 1, 2$) refers to horizontal coordinates (x, y) and the mean vertical velocity is assumed equal to zero. After time averaging, (1) can be simplified with the aid of the following assumptions: (1) straight and parallel contours, e.g., $(\partial/\partial y)(\overline{\ }) = 0$ (overbar indicates time averaging); (2) steady state conditions, i.e., $(\partial/\partial t)(\overline{\ }) = 0$; (3) wave-induced and turbulent velocity components are statistically independent (uncorrelated), i.e., $\tilde{u}\tilde{v} = 0$; and (4) horizontal turbulent momentum flux is small compared to wave induced momentum flux [*Stive and Wind*, 1982], i.e., $(\partial\rho\overline{\tilde{v}\tilde{u}}/\partial x) \ll (\partial\rho\overline{\tilde{v}\tilde{u}}/\partial x)$, and can be neglected. Contributions caused by momentum mixing caused by interactions between cross-shore and longshore currents ($\partial\rho\overline{VU}/\partial x$) are usually not negligible [*Svendsen and Putrevu*, 1994; *Garcez Faria et al.*, 1996]. Nevertheless, they are neglected here for the sake of simplicity. Applying these assumptions, the alongshore momentum equations can be written

$$-\frac{\partial\rho\overline{\tilde{w}\tilde{v}}}{\partial z} = \frac{\partial\rho\overline{\tilde{v}\tilde{u}}}{\partial x} + \frac{\partial\rho\overline{\tilde{w}\tilde{v}}}{\partial z} \tag{2}$$

which says that the sum of cross-shore changes in the wave-induced alongshore momentum flux and vertical changes in the wave-induced Reynolds stress are balanced by vertical changes in alongshore turbulent shear stress.

Applying a first-order turbulence closure, the alongshore turbulent shear stress can be defined

$$\tau_y(z) = -\rho\overline{\tilde{w}\tilde{v}} = \rho\mu_t\frac{\partial V}{\partial z} \tag{3}$$

where μ_t is the turbulent eddy viscosity, which is assumed to be uniform with depth. Substituting (3) into (2)

$$\frac{\partial\tau_y(z)}{\partial z} = \frac{\partial\rho\overline{\tilde{v}\tilde{u}}}{\partial x} + \frac{\partial\rho\overline{\tilde{w}\tilde{v}}}{\partial z} \tag{4}$$

The cross-shore gradient of $\overline{\tilde{v}\tilde{u}}$ is constant in the alongshore direction for straight and parallel contours. Within the surf zone the shallow water approximation holds; thus $\overline{\tilde{v}\tilde{u}}$ is assumed independent of depth. The wave-induced Reynolds stress term ($\overline{\tilde{w}\tilde{v}}$) can arise from sloping bottom effects as well as from wave amplitude gradient effects, and it would have a nonzero contribution even for linear wave theory [*Deigaard and Fredsoe*, 1989]. Nevertheless, *Rivero and Arcilla* [1995] showed that $\overline{\tilde{w}\tilde{v}}$ is a linear function of depth, and hence its; vertical gradient is a constant. Consequently, the right-hand side of (4) is independent of depth, and the shear stress profile is determined by integrating (4) over depth to give

$$\tau_y(z) = [\tau_y(0) - \tau_y(-h)]\frac{z}{h} \tag{5}$$

Linearly varying shear stress occurs in flows driven by uniform hydrostatic pressure gradients, such as in steady open channel flows, which are well described by a logarithmic velocity profile. Therefore it is hypothesized that a steady, uniform, turbulent boundary layer flow over a rough surface in the alongshore direction can be described by a logarithmic profile

$$V(z) = \frac{v_*}{\kappa}\ln\left(\frac{z+h}{z_0}\right) \tag{6}$$

where z is positive upward from the surface, h is the mean water depth, κ is the Von Karman constant (0.4), v_* is the alongshore shear stress velocity, and z_0 is the physical roughness height, determined by bottom topography and sediment grain size. When waves are present, nonlinear interactions between waves and currents within the bottom boundary layer increase the bottom shear stress. Following *Grant and Madsen* [1979], this additional stress can be modeled by an apparent roughness height z_a, that is analogous to, but larger than z_0.

The mean bottom shear stress $[\overline{\tau_y(-h)}]$ is related to the longshore shear stress velocity (v_*) through

$$\overline{\tau_y(z = -h)} = \rho v_*^2 \tag{7}$$

In addition, a bed shear stress coefficient, C_f, can be calculated assuming a quadratic bed shear stress relationship

$$\overline{\tau_y(-h)} = \rho C_f\overline{(u^2 + v^2)^{1/2}v} \tag{8}$$

and combining with (7) gives

$$C_f = \frac{v_*^2}{\overline{(u^2 + v^2)^{1/2}v}} \tag{9}$$

which includes contributions from both steady (U, V) and nonsteady ($\tilde{u}$, $\tilde{v}$, $\acute{u}$, $\acute{v}$) velocity components.

2.2. Surface Layer

The surface layer is governed by waves and wind. Wave effects are manifested in three ways: (1) an undulating boundary is imposed on a mean current, which is being measured in an Eulerian frame; (2) the mass transport velocity in the crest-trough region caused by obliquely incident waves contributes to the longshore flow; and (3) turbulence generated by breaking waves modifies the mean velocity profile and the eventual contribution of wave rollers to the mass transport.

The shape of the mean current profile in this layer is determined mostly by the fact that the current meter is intermittently in and out of the water in the wave crest-trough region; for example, for a linear wave the current meter is out of the water half the time at the mean sea level (msl), and the time-averaged current is only 50% of the expected value from the logarithmic profile. To account for this, the surface elevation probability density function (pdf) is applied to the expected mean current profile in the absence of waves. The percent of time the current meter is in the water is given by $1 - P(\eta)$, where $P(\eta)$ is the cumulative surface elevation pdf. In an Eulerian frame of reference the modified mean current within the surface layer is given by

$$V(z) = [1 - P(\eta)]V'(z) \tag{10}$$

where $V'(z)$ represents the logarithmic profile in the absence of waves (6). For moderate wave conditions in deep water the surface elevation pdf is well described by the Gaussian pdf. As will be seen, the measured pdf values in the surf zone are slightly positively skewed from the Gaussian distribution.

The mass transport velocity associated with obliquely incident waves can contribute to the longshore flow in the upper layer. Assuming irrotational flow, the mass flux (transport) in the direction of wave transport, M, can be evaluated by considering separately two regions in an Eulerian frame of reference [*Philips*, 1977]. In the first region, from the bottom to the msl, the contribution is zero for irrotational flow. Within the second region, from the msl to the water surface (η), $\tilde{u}$ is not defined for linear wave theory. A Taylor series expansion about $z = 0$ is used to extend defined values of $\tilde{u}(0)$ at the

surface, giving a second-order approximation to M. The mass transport for a single wave is interpreted to this order, in an Eulerian reference frame, as due to a uniform velocity confined to the crest-trough region. Applying linear wave theory, a mass transport velocity is defined by

$$U = \frac{M}{\rho(2A)} \tag{11}$$

where A is the wave amplitude.

For random waves the wave amplitudes can be described by the Rayleigh distribution to a first approximation, even within the surf zone [*Thornton*, 1979]. The only waves that contribute at any elevation, z, will have an amplitude $A \geq |z|$. Assuming directionally narrow banded waves, the ensemble-averaged mass transport velocity profile in the direction of wave travel is obtained by applying the wave amplitude probability density function

$$\langle U(z) \rangle = \int_{|z|=A}^{\infty} U(A)p(A)\, dA \tag{12}$$

where angle brackets represent ensemble averaging. The Rayleigh probability density function is given by

$$p(A) = \frac{8A}{H_{\text{rms}}^2} e^{-(2A/H_{\text{rms}})^2} \tag{13}$$

where $0 < A < h$ and H_{rms} is the root-mean-square (rms) wave height. Substituting (13) back into (12), applying linear wave theory, and performing the integration give

$$\langle U(z) \rangle = \frac{\omega}{8} \frac{H_{\text{rms}}}{\tanh kh} \left[\frac{2|z|}{H_{\text{rms}}} e^{-(2|z|/H_{\text{rms}})^2} + \frac{\sqrt{\pi}}{2} \operatorname{erfc}\left(\frac{2|z|}{H_{\text{rms}}} \right) \right] \qquad |z| < h \tag{14}$$

where erfc (x) is the complementary error function, ω is the wave radial frequency, and k is the radial wavenumber. The alongshore component of the mass transport velocity is defined by

$$\langle V(z) \rangle = \langle U(z) \rangle \sin \bar{\theta} \tag{15}$$

where $\bar{\theta}$ is the mean incident wave angle with respect to the beach normal for the assumed directionally narrow banded waves.

The mean longshore current within the surface layer, as observed in an Eulerian reference frame, is modeled by adding the corrected logarithmic profile for the cumulative surface elevation pdf (10) with the alongshore component of the mass transport velocity (15)

$$V_{\text{sfc}}(z) = [1 - P(\eta)]V'(z) + \langle U(z) \rangle \sin \bar{\theta} \tag{16}$$

3. DUCK94 Experiment

The measurements described here are part of the comprehensive nearshore DUCK94 experiment conducted during October 1994 at the U.S. Army Corps of Engineers Field Research Facility (FRF), Duck, North Carolina. The FRF is located on the Outer Banks, a barrier island formation with no major coastal structures to obstruct nearshore flows. The beach is a two-bar system with a dynamic inner bar (30–120 m offshore) and a secondary bar with lower amplitude (300–400 m offshore). The mean foreshore slope of the beach is ~0.08 (1:12), and the slope offshore of the bars is ~0.006 (1:170) [*Lippmann et al.*, 1993]. The mean tidal range is 1.0 m. Sediments within the surf zone are well sorted with a mean grain size of 0.2 mm. Sediments on the foreshore are poorly sorted with larger mean grain size (>0.4 mm).

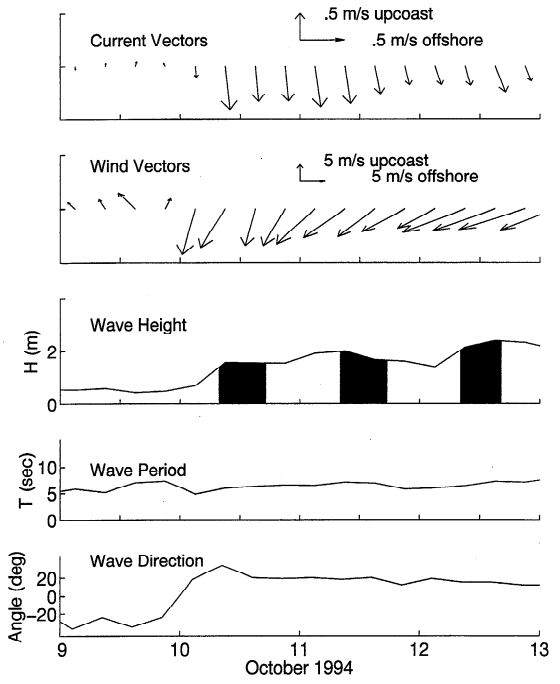

Figure 1. Climatology for the 3 days considered (October 10, 11, and 12). Currents were measured in the middle of the trough. H is the significant wave height, T is the period of peak frequency, and Angle is the mean wave angle relative to beach normal (θ).

The data analysis presented is for the October phase of the DUCK94 experiment. The weather during October was climatologically characterized by three distinct phases: weak currents and winds from north (October 4–9), relatively strong currents from north (0.6–1.0 m s^{-1}) caused by a storm with predominant winds and waves from north (October 10–17), and variable currents and winds from north/south (October 17–21). For the first phase (October 4–9) the currents were weak and barely above sensor accuracy. During the last phase (October 17–21), currents and winds were highly variable, and a hole developed in the bar associated with a rip current system (observed with dye), such that the basic assumptions of steady state and straight and parallel contours are violated. Within the second phase (October 10–17), observations were limited because of the Coastal Research Amphibious Buggy (CRAB) not being able to operate during the height of the storm on October 15 and being limited to the area inside the bar on October 13, 14, 16, and 17 because of large waves. Therefore the data selected for analysis are from October 10–12 (Figure 1) during the strong longshore currents period when observations spanned the entire surf zone and conditions approximate the assumptions of steady state and straight and parallel contours. Within this period a logarithmic profile is well defined.

A specially designed sled was used as a platform to mount instruments (Figure 2). The sled is constructed of a 3 × 4 m, 6 inch aluminum pipe frame with two 5 m length, 20 cm diameter

Figure 2. Photograph of the sled being pulled off the beach by the Coastal Research Amphibious Buggy (CRAB) (upper right) during DUCK94 experiment. Vertical array of electromagnetic current meters (ems) are mounted along the sled mast (center left).

pipe runners. This low-profile structure was stabilized by 180 kg of lead weight plus ~450 kg of sand inside the runners. In addition, there were four fins (45 cm wide) extending 60 cm into the sand to insure that the sled did not move while on station.

Currents were measured using a vertical stack of eight Marsh-McBirney two-component electromagnetic current meters (ems) with 2.5 cm diameter spherical probes mounted along a 2.5 m mast (Figure 2). The ems elevations above the bed were 23, 42, 68, 101, 147, 179, 224, and 257 cm. The ems were displaced at least 1 m from the sled, and the sled was oriented such that the vertical stack of ems was on the "up-current" side of the sled to avoid flow contamination by the sled structure during observations. The ems were precalibrated and postcalibrated in a tow tank at the Naval Postgraduate School with an agreement of 1.9% in gain. An in situ determination for the offset is used, which was obtained by reversing the orientation of the ems on a very slow longshore current day (October 8) by turning the sled around and returning it to the same location (within 1 m) within 1 hour. The in situ determined offsets were within 1 cm s^{-1}.

The sled orientation was determined using a digital compass mounted on the sled with accuracy O(1°). Measured two-component velocities were reduced to a shore normal right-handed coordinate system (positive offshore and to the south) by using compass data and adding at each sled position any deviation of the contour line, as measured by the CRAB, from a shore parallel direction. Velocity errors associated with the rotation of the coordinate system were comparable to the determined offsets and therefore were neglected.

Waves and mean water level were measured using an array of five pressure sensors configured in a 3 m square with sensors at each corner and one in the center. The data were digitally encoded on the sled to 14 bit precision at 36 samples s^{-1} and transmitted to shore via a fiber-optic cable, where signals were monitored and recorded. Short cables from the sensors to the data acquisition system on the sled (<7 m) resulted in low noise ems and pressure sensor signals. An armored cable, married to the sled chain tether, provided power and controller signals for the instruments via two conductors and returned the digitized signals and video via a fiber-optic line.

The sled was towed to the farthest offshore location for the first run (~160 m from the shoreline) by the 11 m high, motorized, three-wheel CRAB. A four-wheel drive forklift pulled the sled shoreward 10–30 m for subsequent measurement runs that are referred to in the text by sequential numbers within each day. Five to eight runs were made across a transect each day, and each run was nominally 1 hour. The data were acquired during daylight to early night, which happened to span the high tide during this period.

The morphology of the bottom (bathymetry) was measured at various scales from the CRAB. Large-scale variations of bathymetry were obtained by using an autotracking laser ranging system to measure the CRAB position approximately every meter with a vertical accuracy of <3 cm rms. Small-scale vertical bottom variations relative to the CRAB, including ripples and megaripples, were measured with a 1 MHz sonic altimeter mounted on the CRAB, 70 cm from the bed. The altimeter has a 3.4° beam width which translates into an ~4 cm footprint and a nominal sampling rate of 25 Hz, which resulted in a sample spacing of 2–4 cm (dependent on CRAB speed) with millime-

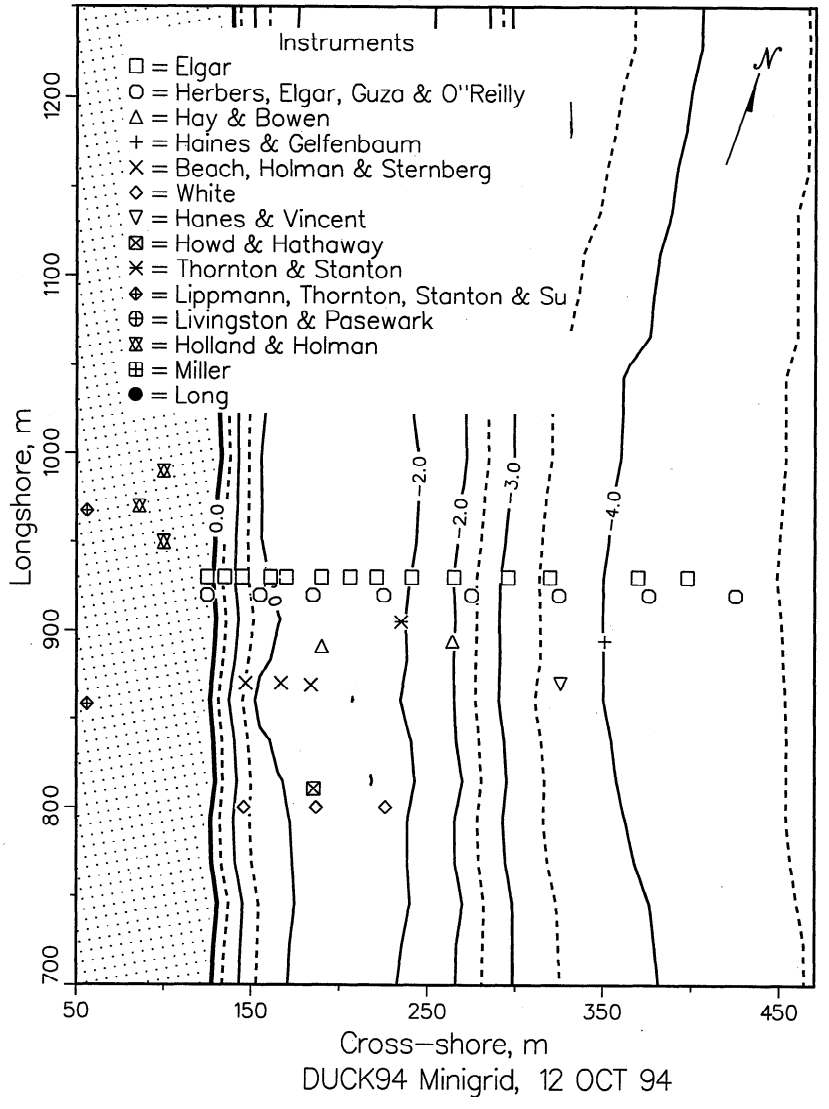

Figure 3. Bathymetry during DUCK94 experiment (October 12). The sled transect line (~910 m alongshore) is indicated by a horizontal line with an asterisk at the 2 m contour line intercept.

ter vertical resolution and accuracy <2 cm [*Gallagher et al.*, 1996]. The decrease in accuracy relative to resolution is due to the changing reflective surface owing to the bed dialating or sediment transported along the bed as waves pass overhead. The CRAB survey and altimeter measurements were combined to obtain a high-resolution description of the bottom [*Thornton et al.*, 1997]. Contour plots of the bathymetry for the days selected for analysis show the alongshore contours in the vicinity of the sled measurements to be essentially straight and parallel (Figure 3; October 12 is typical). Bathymetry for the three selected days (Figures 4a, 5a, and 6a) shows a pronounced bar progressively moving offshore and significant small-scale morphology in the trough. Areal variations were determined using a 500 kHz side-scan sonar also mounted on the CRAB. Meteorological information of wind, air temperature, atmospheric pressure, and sea surface temperature were recorded simultaneously at the seaward end of the 600 m long FRF pier and atop the FRF building in front of the pier.

4. Data Results

The data are qualitatively sorted by location into the two regions of over the bar and in the trough. This sorting allows a better identification of the possible correlations among variables, as wave breaking, which is a major controlling factor within the surf zone, significantly changes for these regions.

Since the logarithmic velocity profile hypothesis is a bottom boundary layer concept, information from ems near the surface influenced by the effects of waves and wind as well as from coming in and out of the water are not included. A criterion is established such that only data from ems below (msl $- H_{rms}$) are considered to define the logarithmic profile of the bottom boundary layer. This criterion assures that the ems used in the analysis came out of the water <0.25% of the time based on a Gaussian distribution, which is conservative for the measured positively skewed distributions.

The rms wave height is approximated by $H_{rms} = \sqrt{8\sigma^2}$, where σ^2 is the variance calculated from the surface elevation time series. Surface elevation was calculated by Fourier transforming a 1-hour pressure record, applying a linear wave theory transfer function to the complex Fourier amplitudes in the frequency domain, and inverse transforming to obtain the surface elevation time series [*Thornton and Guza*, 1982].

All 22 vertical profiles of longshore currents obtained during these 3 days are analyzed. The profiles are based on the mea-

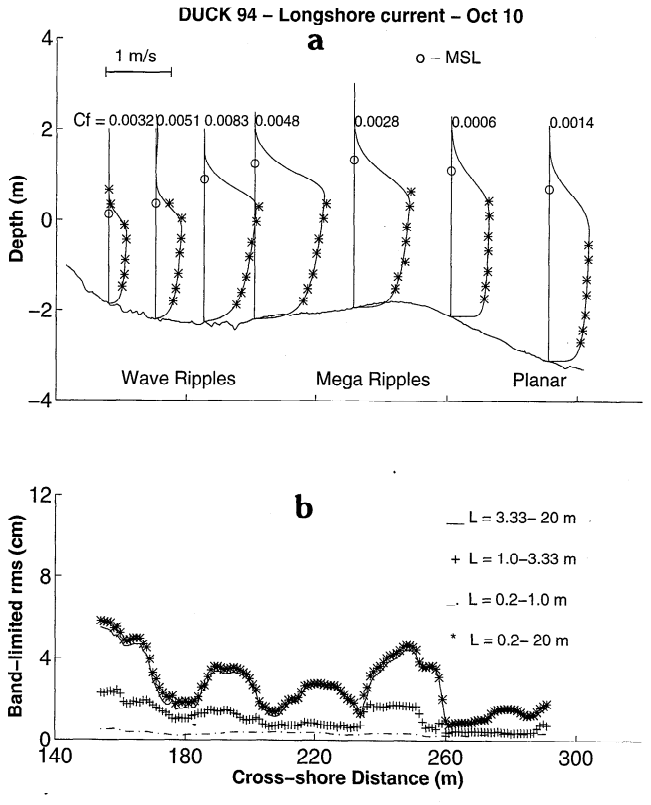

Figure 4. (a) Measured (line with asterisk) and predicted (line) vertical profiles of mean longshore currents superposed on bottom profile with tide elevation indicated by an open circle and measured C_f values. (b) Variation of band-limited root-mean-square (rms) bottom roughness with cross-shore distance for October 10.

surements by four to seven ems over the vertical. The em closest to the sea bed was not used because of malfunction. Mean alongshore velocities are 1-hour averaged data with the exception of three runs: run 7 on October 11 and runs 6 and 7 on October 12, which are 40 min averaged data. In examining the bottom boundary and surface layers the ems data are treated separately.

For the bottom boundary layer, logarithmic profiles are fit to the data based on a linear regression least squares method. The value of z_a is calculated from the z intercept of the linear regression on a semilog plot of z versus $V(z)$, and the shear stress velocity v_* is calculated from the slope.

C_f values are calculated using measured velocities (u, v) in (9), time averaged over the record length, with v_* determined by least squares fit. C_f values are dependent on the elevation of the measured u, v values. Typically, C_f is calculated using measured u, v values referenced to 1 m above the bed. A sensitivity analysis on the variation of C_f to the elevation of the selected gage was performed, showing that the variation of C_f was dominated by the time-averaged alongshore velocity (V). This term was not only the largest in the denominator of (9) but also varied the most with depth. Therefore, to minimize the depth dependence of C_f, the depth-averaged velocity calculated from the logarithmic velocity profile $\{V_d = (v_*/\kappa)\,[\ln (h/z_a) + (z_a/h) - 1]\}$ is used to specify the dominant time-averaged alongshore velocity. The em located at the elevation of 1 m above the bed is used to measure the smaller terms (total cross-shore velocity u and the nonsteady component of the alongshore velocity $\bar{v} + \acute{v} = v - V$), which have weak vertical variation outside the bottom boundary and surface layers. The total alongshore velocity is obtained by adding V_d to the measured nonsteady component $\bar{v} + \acute{v}$. The use of this method resulted in a mean variation of C_f with depth of only 7% with a standard deviation of 6% and a maximum variation of 24%, provided the gage used to measure the cross-shore velocity and nonsteady component of the alongshore velocity was not in the surface layer ($z >$ msl $- H_{\text{rms}}$). Calculated C_f, z_a, and v_* values are listed in Table 1.

Error estimates of z_a and v_* based on the linear regression correlation coefficients (C) are calculated using [*Gross and Nowell*, 1983; *Cacchione et al.*, 1987]

$$v_* \pm v_* t_{(n-2,1-\alpha/2)} \left(\frac{C^{-2} - 1}{n - 2} \right)^{1/2} \tag{17}$$

$$\ln z_a \pm t_{(n-2,1-\alpha/2)} \left\{ \frac{1}{n} \sum_{i=1}^{n} [\ln (z_i)]^2 \right\}^{1/2} \left(\frac{C^{-2} - 1}{n - 2} \right)^{1/2} \tag{18}$$

where n is the number of ems used for the regression and $t_{(n-2,1-\alpha/2)}$ is the Student's t distribution for $(1 - \alpha)$ confidence interval with $(n - 2)$ degrees of freedom.

The uncertainties of C_f values can be determined from the error estimates of v_* and the time and depth-averaged velocity calculated from the measurements $V_m = (1/h) \int_{-h+z_a}^{0} [(v^2 + u^2)^{1/2} v]^{1/2}\, dz$ (mean velocity, hereafter)

$$C_f \pm C_f \left[\frac{1 + 2v_{*_{\text{err}}} + (v_{*_{\text{err}}})^2}{1 + 2V_{m_{\text{err}}} + (V_{m_{\text{err}}})^2} - 1 \right] \tag{19}$$

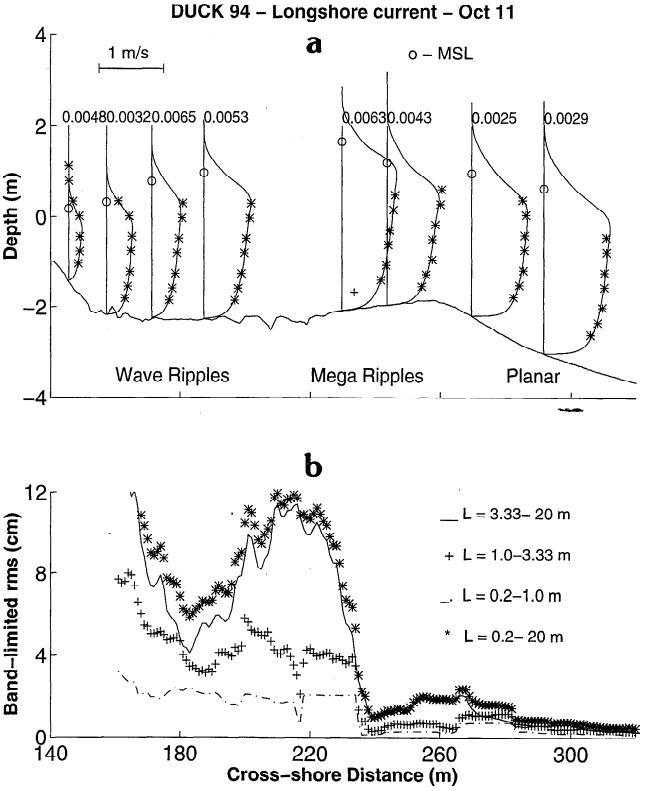

Figure 5. Same as in Figure 4 but for October 11. The anomalous measurement point (plus) in the fourth run (Figure 5a) is not included in the linear regression.

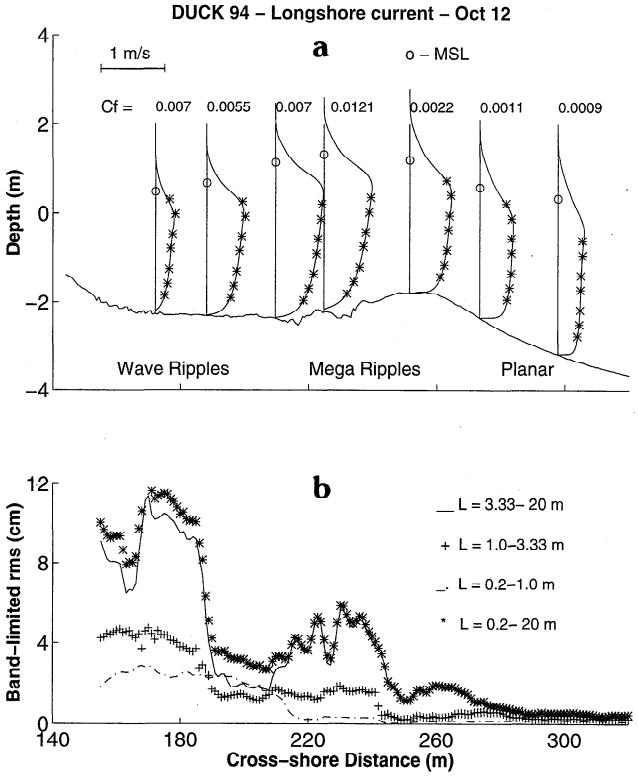

Figure 6. Same as in Figure 4 but for October 12.

where $v_{*_{\mathrm{err}}}$ is the relative error of the shear stress velocity at a given confidence level calculated from (17) and $V_{m_{\mathrm{err}}}$ is the relative error of the mean velocity determined by $V_{m_{\mathrm{err}}} = (1\ \mathrm{cm\ s^{-1}}/V_m)$, assuming that the mean velocity has a constant absolute error equal to the in situ determined offset (1 cm $\mathrm{s^{-1}}$). Error estimates for C_f, z_a, and v_* are listed in Table 2 for a 95% confidence interval.

The measured cumulative surface elevation pdf is used to describe the surface layer and compares reasonably well with the Gaussian cumulative pdf (Figure 7). The Gaussian distribution has zero skewness and kurtosis equal to three. The measured skewness values ranged from 0.26 to 0.57, and kurtosis values ranged from 2.7 to 3.5, indicative of weakly nonlinear waves.

In the surface layer the upper ems sometimes came in and out of water, which causes noise in the ems outputs. To eliminate this noise, the current velocities were set to zero when the ems were within 5 cm of the surface as determined from the surface elevation time series.

The combined surface and bottom boundary layer solution is the logarithmic profile given by (6) from z_a up to (msl $- H_{\mathrm{rms}}$) and the modified logarithmic profile by the observed cumulative surface elevation pdf plus the alongshore component of the mass transport velocity given by (16) above this level. As a typical example, the profile for the seventh run of October 10 is enlarged in Figure 8, where the solid line is the logarithmic profile and the dashed line the modified profile within the surface layer.

The observed and model-predicted velocity profiles at successive offshore positions (runs) that the sled occupied during a transect are shown in Figures 4a, 5a, and 6a. The largest deviation occurs for the fourth run of October 11, which generates an outlier in the parameter estimates if the data from the cm at an elevation of 42 cm above the sea bed (Figure 5a) is included in the linear regression. A comparative analysis for all ems for this run showed the energy density spectra to be nearly uniform (average variance of 0.072 $\mathrm{m^2}$ and standard deviation of 0.013 $\mathrm{m^2}$) with exception of this em (variance of 0.021 $\mathrm{m^2}$). Thus data from this em is disregarded, and a new

Table 1. Logarithmic Profile Fitting Results

Day	Run	Cross-Shore Position, m	Depth (h), m	Root-Mean-Square Wave Height (H_{rms}), m	$\gamma = h/H_{\mathrm{rms}}$	Root-Mean-Square Bottom Roughness (r), cm	Apparent Roughness Height (z_a), cm	Shear Stress Velocity (v_*), cm $\mathrm{s^{-1}}$	Bed Shear Stress Coefficient (C_f)	Skin Friction Shear Stress Velocity (v_{*_s}), cm $\mathrm{s^{-1}}$
10	1	291	3.80	1.11	0.29	1.8	0.02	2.6	0.0014	1.5
10	2	261	3.24	1.12	0.35	0.8	0.0002	1.7	0.0006	1.1
10	3	231	3.26	1.15	0.35	2.0	0.3	5.1	0.0028	2.8
10	4	201	3.45	0.89	0.26	2.7	0.6	7.1	0.0048	3.9
10	5	185	3.18	0.75	0.24	2.6	2.4	7.0	0.0083	3.9
10	6	170	2.57	0.63	0.25	3.3	1.4	3.2	0.0051	1.6
10	7	156	1.98	0.55	0.28	5.8	0.3	1.8	0.0032	0.7
11	1	292	3.66	1.30	0.36	0.8	0.2	5.6	0.0029	5.5
11	2	270	3.16	1.27	0.40	1.8	0.2	4.7	0.0025	2.5
11	3	244	3.16	1.12	0.35	1.3	0.9	5.6	0.0043	4.0
11	4	230	3.75	0.98	0.26	7.4	1.5	6.3	0.0063	3.0
11	5	187	3.24	0.89	0.27	6.7	1.1	5.2	0.0053	2.4
11	6	171	3.05	0.84	0.28	9.0	3.0	4.0	0.0065	1.7
11	7	157	2.50	0.76	0.30	16.0	0.5	2.7	0.0032	1.1
11	8	146	1.63	0.66	0.40	2.2	3.2	2.3	0.0048	1.1
12	1	298	3.51	1.23	0.35	0.5	0.02	1.6	0.0009	1.0
12	2	273	2.93	1.30	0.44	1.1	0.02	2.3	0.0011	1.5
12	3	252	2.98	1.21	0.41	1.2	0.2	3.6	0.0022	2.2
12	4	225	3.54	1.04	0.29	4.2	6.9	8.1	0.0121	5.0
12	5	210	3.51	0.97	0.28	3.3	2.3	6.1	0.0069	3.7
12	6	188	2.99	0.90	0.30	6.3	1.8	4.7	0.0055	2.2
12	7	172	2.74	0.84	0.31	11.0	6.8	3.2	0.0073	1.3

Table 2. Ninety-Five Percent Confidence Bands on v_*, z_a, and C_f

Day	Run*	Number of ems Used for the Regression (n)	Student's t Distribution ($t_{(n-2.1-\alpha/2)}$)	Correlation Coefficient Between Observations and Log-Profile Predictions (C)	95% Confidence Band		
					Shear Stress Velocity (v_*), %	Apparent Roughness Height (z_a)	Bed Shear Stress Coefficient (C_f), %
10	1	7	2.015	0.983	17	2.3	33
10	2	5	2.353	0.953	43	7.2	99
10	3	5	2.353	0.952	44	7.4	102
10	4	6	2.132	0.992	14	1.9	27
10	5	6	2.132	0.992	13	1.9	26
10	6	5	2.353	0.999	5	1.3	6
10	7	4	2.920	0.991	28	3.5	56
11	1	6	2.132	0.969	27	3.6	58
11	2	5	2.353	0.963	38	5.8	87
11	3	5	2.353	0.975	31	4.1	68
11	4	6	2.132	0.987	17	2.4	35
11	5	6	2.132	0.991	15	2	28
11	6	5	2.353	0.998	9	1.5	14
11	7	5	2.353	0.996	12	1.8	21
12	1	6	2.132	0.966	29	3.9	59
12	2	4	2.920	0.968	53	10	128
12	3	5	2.353	0.989	20	2.5	41
12	4	6	2.132	0.998	6	1.3	10
12	5	6	2.132	0.997	8	1.5	14
12	6	5	2.353	0.995	14	1.9	25
12	7	5	2.353	0.992	17	2.2	30

Confidence limits are found by multiplying and dividing z_a by factor.
*Eighth run of October 11 is not included as only two electromagnetic current meters (ems) are used for profile fitting.

regression is calculated with the remaining six ems. This procedure eliminates the outlier.

5. Discussion

Three days of the DUCK94 experiment are examined when strong longshore currents occurred. Mean longshore current profiles obtained using four to seven ems spaced from 42 to 257 cm above the sea bottom are used to test the validity of the logarithmic profile hypothesis within the energetic surf zone region.

5.1. Bottom Boundary Layer

A high correlation coefficient for the linear regression is commonly accepted as an indicator of the validity of the logarithmic approach [*Grant et al.*, 1984; *Gross et al.*, 1994; *Li*, 1994]. The linear correlation coefficients for all profiles ranged from 0.95 to 0.99 (Table 2), with an average value of 0.98, and the largest deviations occurring over the bar where wave break-

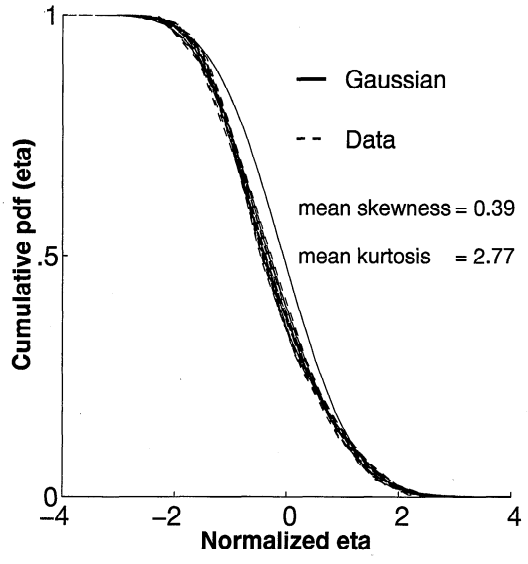

Figure 7. Comparison between measured and Gaussian cumulative surface elevation probability density function (pdf) for all the runs during the 3 days considered (October 10, 11, and 12). Mean skewness and kurtosis for the 3 days are indicated.

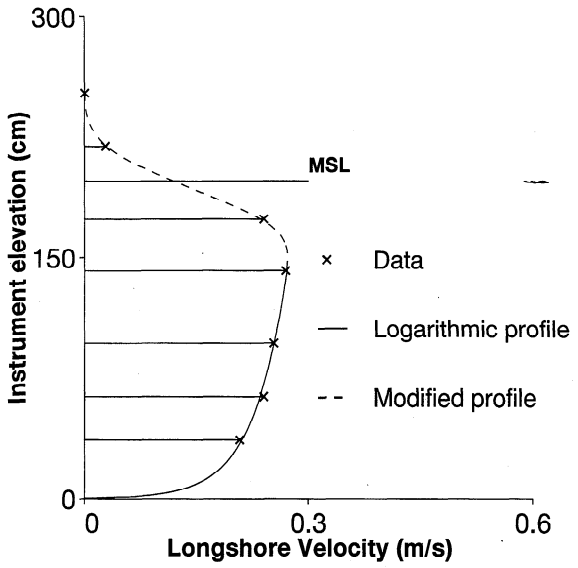

Figure 8. Vertical profile combining bottom boundary and surface layer models for the seventh run of October 10. The upper three ems sometimes were out of the water.

Table 3. Sensitivity of the ems to the Elevation From the Bed as Inferred From the Zero-Shifting Method

Day	Run	Number of ems Used for the Regression (n)	Zero Shift, cm	Correlation Coefficient Between Observations and Log-Profile Predictions (C)	95% Confidence Band: Shear Stress Velocity (v_*), %	95% Confidence Band: Apparent Roughness Height (z_a), $\times/\div$
10	7	3	0	0.985	72	2.1
10	7	3	−1	0.986	66	2.0
10	7	3	−2	0.986	60	2.0
10	7	3	−3	0.986	55	2.0
10	7	3	−4	0.987	49	1.9
10	7	4	−5	0.991	31	1.8
10	7	3	5	0.984	107	2.2
11	7	4	0	0.993	87	3.0
11	7	4	−1	0.994	81	2.9
11	7	4	−2	0.994	75	2.9
11	7	4	−3	0.994	69	2.8
11	7	4	−4	0.994	64	2.8
11	7	5	−5	0.996	53	2.7
11	7	4	5	0.992	124	3.2
12	3	4	0	0.987	37	4.1
12	3	4	−1	0.988	34	4.1
12	3	4	−2	0.988	31	4.0
12	3	5	−3	0.988	20	3.7
12	3	5	−4	0.988	19	3.7
12	3	5	−5	0.989	17	3.6
12	3	4	5	0.985	56	4.4

Confidence limits are found by multiplying and dividing z_a by factor.

ing was strong. Anomalous high correlation coefficients can be obtained for profiles calculated using a small number of ems for the linear regression, such as occurred for stations very close to the shoreline because of shallow water. Thus a high correlation coefficient, although necessary, is not sufficient to validate the logarithmic profile approach.

Other measures of how well the logarithmic model describes the mean alongshore current profile within the bottom boundary layer are the uncertainties of the calculated shear stress velocity v_* (17) and apparent roughness height z_a (18). These uncertainties reflect both the correlation coefficients and the number of ems used in the regression. An example is comparing the fourth run of October 11 with the seventh run of October 10 (Table 2). The latter has a higher correlation coefficient (0.991), but only 4 ems were used in the linear regression; thus uncertainties in the calculated v_* and z_a values are larger for this run, even though the former has a lower correlation coefficient (0.987). Therefore the uncertainties are not biased by an anomalous high correlation coefficient due to a small number of ems used in the regression. The degenerate case is when only two ems are used for the linear regression (eighth run of October 11), resulting in a correlation coefficient of one, which does not allow the calculation of the uncertainties for v_* and z_a. Consequently, data from this run are disregarded.

There is some uncertainty of the exact distance of the ems from the bed because the sled runners sank an unknown depth into the sand, depending on the bearing capacity of the bed (theory and divers suggest 3–8 cm) and owing to the undulating bottom, particularly over megaripples. To test the sensitivity of the logarithmic profile due to the uncertainty in elevation, the elevation of the ems was shifted ±5 cm in steps of 1 cm, and the linear regression least squares fit was recalculated until the best correlation between the data and the logarithmic model predictions was obtained for each run [*Grant et al.*, 1984].

As the bathymetry is not uniform over the transect covered by the sled, no unique zero-shift value should be expected to optimize the correlation coefficient for all runs. Another effect on the error calculation to be considered with an ad hoc decrease (increase) in the elevation of the ems is that an em previously located above (below) the model cutoff level (msl − H_{rms}) can be relocated to a new elevation below (above) this level. For example, an em previously neglected by the model is now included in the linear regression. The zero-shifting modifies the error estimates of v_*, z_a, and C_f (17)–(19) by changing the correlation coefficients and the number of ems used for the regression.

With the uncertainties involved the zero-shifting method was only applied whenever a significant reduction (>10%) was obtained in the shear stress velocity error estimate. Applying this criteria, only three runs were shifted (by the same, 5 cm): the seventh runs of October 10 and 11 and the third run of October 12. The sensitivity of the ems to elevation from the bed as inferred from the zero-shifting method for these three runs is shown in Table 3. The general trend is that both the shear stress velocity and apparent roughness height errors decreased with increased negative shift, although the improvement is only significant for the shear stress velocity. The values listed in Tables 1 and 2 for these runs were calculated after applying the zero shift.

The observed and model-predicted velocity profiles at successive offshore positions (runs) that the sled occupied during a transect are shown in Figures 4a, 5a, and 6a. The data agree well with the model indicating that the contribution from momentum mixing arising from interactions between cross-shore and longshore currents ($\partial \rho \overline{VU}/\partial x$) neglected for the sake of simplicity does not significantly modify the vertical profile of

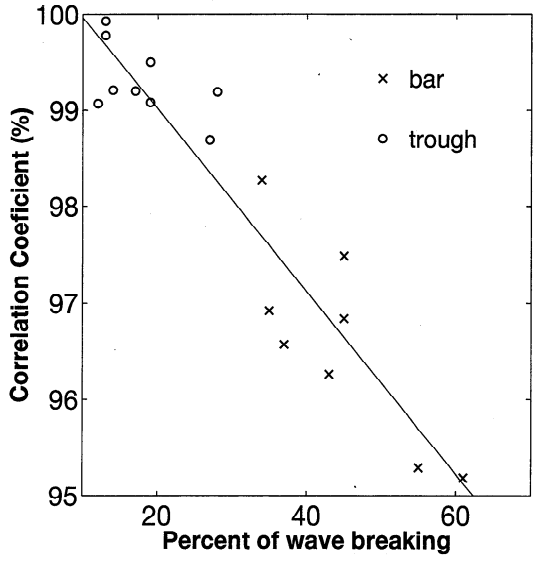

Figure 9. Correlation coefficient between observations and logarithmic profile predictions versus percentage of wave breaking calculated from video data. The line represents a linear regression with a regression coefficient of −0.94.

longshore currents, suggesting that $(\partial \rho \overline{VU}/\partial x)$ is independent of depth.

The largest discrepancies between measured and modeled profiles occur over the bar, where wave breaking is most intense (x distance between 220 and 240 m). The surface layer during wave breaking is typified by an intense production of turbulence that eventually is dissipated in the shear layer at the lower boundary of the surface roller for spilling type breakers and more intense injection of turbulence for plunging type breakers. The increase of turbulent mixing caused by wave breaking produces a more uniform vertical profile of the mean longshore current within the bottom boundary layer for a given bottom shear stress, compared with profiles in the absence of breaking. Therefore larger discrepancies between observations and logarithmic profile predictions (lower correlation coefficients) would be expected for increased turbulent mixing caused by wave breaking.

To test this hypothesis, percentages of waves breaking were determined from video recordings. The number of waves breaking is determined using the methods of *Lippmann and Holman* [1989], while the total number of waves is found applying the zero-upcrossing method to the surface elevation time series (for details, see T. C. Lippmann and E. B. Thornton, The spatial distribution of wave breaking on a barred beach, submitted to *Journal of Geophysical Research*, 1997). The general decrease of the correlation coefficient between observations and logarithmic profile predictions with increasing percentage of wave breaking (Figure 9) supports this conclusion.

5.2. Surface Layer

The mean current profile within the surface layer is modified in the presence of winds and waves. The winds act directly to generate longshore currents via the alongshore surface wind stress component and indirectly by generating obliquely incident waves which then force the longshore currents via changes in the radiation stress. *Whitford and Thornton* [1993] measured the various terms in the alongshore momentum balance including wind stress and wave forces during the SUPERDUCK experiment (October 15–18, 1986) at the same location as the DUCK94 experiment. They found an average wind force to wave force ratio for this 4 day period of 0.11 (range 0.02–0.33) for a mean alongshore component of wind speed of 3.6 m s^{-1} (range 1.9–5.3 m s^{-1}). During the 3 day period studied here the mean alongshore wind speed was 9.3 m s^{-1} (range 7.4–12.1 m s^{-1}) resulting in an average wind force to wave force ratio of 0.21 (0.10–0.50). Despite the wave force dominance characterizing wave-driven longshore currents, the wind force contribution is not negligible.

Winds and currents are approximately from the same direction (Figure 1); thus the wind force effect is to increase the alongshore currents. As the logarithmic profiles are fit to the data based on a linear regression least squares method, the direct wind force effect is already included in the logarithmic profile. The indirect wind force effect of wave generation resulting in increased wave heights (higher H_{rms} values) is also included in the alongshore component of mass transport velocity. The theoretical exponential decay of wind-induced current speed with depth was not observed within the surface layer due to the dominant effect of the ems intermittently being out of the water and therefore is not included in the model.

The modification of the mean current profile within the surface layer is modeled here by correcting the logarithmic profile predictions for measurements in an Eulerian frame with an undulating boundary and adding the alongshore component of the mass transport velocity (16). As few ems were located above the (msl − H_{rms}) level for each run, a local correlation coefficient as an indicator of the validity of this approach is meaningless. Therefore the validity of the model is evaluated by comparing model predictions with observations for the ensemble of ems located within the surface layer.

The linearity of (16) allows an evaluation of the contribution of each term (intermittent wetting and alongshore component of mass transport velocity) separately. For the intermittent-wetting term only, a plot of predicted versus observed velocities (Figure 10) shows good agreement but with the modified

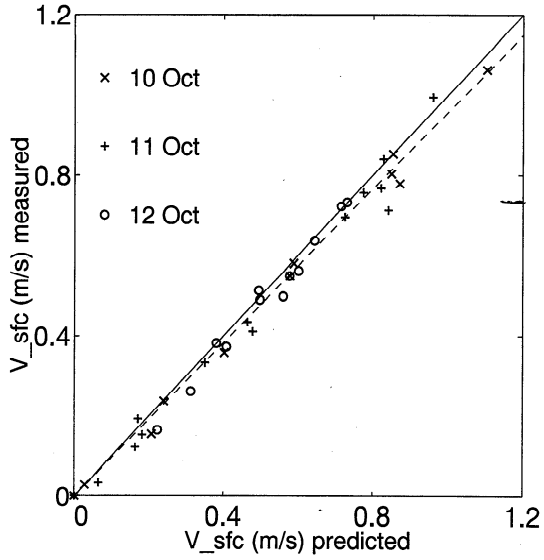

Figure 10. Predicted (10) versus observed longshore velocities within the surface layer. The solid line represents perfect agreement (slope = 1), and the dashed line represents a linear regression with a slope of 0.96.

logarithmic profile by the cumulative surface elevation pdf slightly underpredicting the observed velocities. The rms error and slope of the least squares linear regression between predictions and observations are 13% and 0.96, respectively, giving a slope-error of −4%. Next, including the alongshore component of the mass transport velocity (Figure 11) results in reduced rms and slope errors of 7 and 0.5%. Despite the small magnitude of the mass transport term (on average only 11% of the intermittent-wetting term), its addition corrects the small underprediction of using only (10) and improves the overall agreement with the data by reducing both the rms and slope errors.

Although the results obtained by this first attempt (to the knowledge of the authors) to model mean longshore currents within the surface layer are encouraging, improvements can be achieved by including contributions from at least two physical processes. The first arises from the additional mass transport associated with the presence of wave-breaking generated rollers and will increase the model-predicted velocity within the surface layer. The second is associated with the directional spreading of random waves, and it will have an opposite effect, reducing the model-predicted velocity. Preliminary calculations indicate that these terms are of the same order of the mass transport term, and thus an order of magnitude smaller than the intermittent wetting. The good agreement with the data obtained by applying this simple model is attributed to the dominance of the intermittent-wetting term and compensating effects of neglected contributions from the presence of wave rollers and directional spreading.

5.3. Bed Shear Stress Coefficient

The bed shear stress coefficient (C_f) from the quadratic friction model is an important parameter in both nearshore hydrodynamics and sediment transport. The simplest formulation for longshore currents assumes steady state wave conditions and straight and parallel bottom contours and results in an alongshore balance between cross-shore changes in wave-induced momentum (radiation stress, S_{yx}) with the bottom shear stress to give [*Thornton*, 1970]

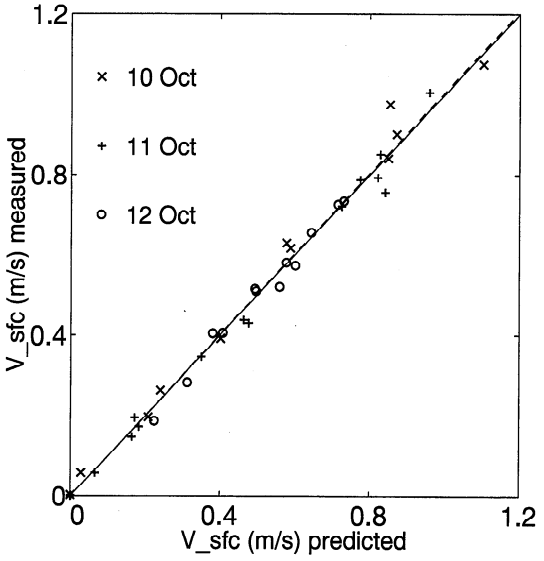

Figure 11. Same as in Figure 10 but including the alongshore component of mass transport velocity (16). The slope of the linear regression is 1.005.

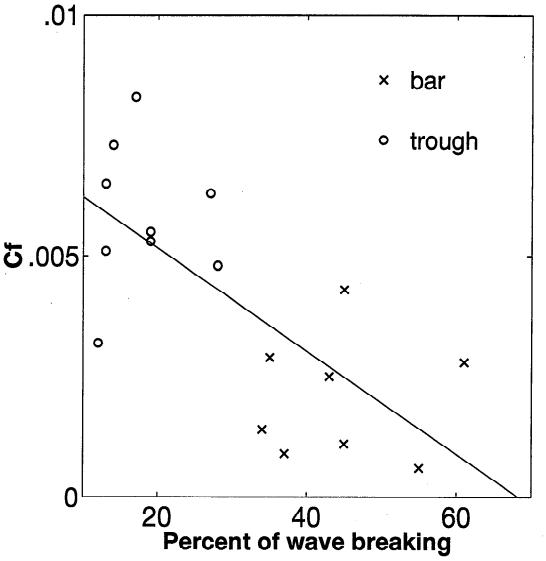

Figure 12. Bed shear stress coefficient (C_f) versus percentage of wave breaking calculated from video data. The line represents a linear regression with a regression coefficient of −0.71.

$$V = \frac{1}{\rho C_f |\mathbf{u}|} \frac{\partial S_{yx}}{\partial x} \tag{20}$$

where $|\mathbf{u}|$ is the magnitude of the total velocity vector. The sediment transport formulation of *Bailard and Inman* [1981], based on the work by *Bagnold* [1966], states that the immersed weight sediment transport rate is proportional to the local rate of energy dissipation

$$\mathbf{i}_t = \rho C_f |\mathbf{u}_t|^3 (\mathbf{K}_{bt} + \mathbf{K}_{st}) \tag{21}$$

where $\mathbf{K}_{bt}$ and $\mathbf{K}_{st}$ are dimensionless time-varying vectors associated with the bedload and suspended load transport rates. It is noted that both the longshore currents and sediment transport rates are direct functions of C_f. Nevertheless, the physical processes governing these phenomena are inherently different. The longshore currents are mainly controlled by form drag of the bed forms and nonlinear interactions between waves and mean current. Sediment transport is mainly related to skin friction caused by sediment grains [*Smith*, 1977; *Dyer*, 1980], although the presence of waves increases the sediment entrainment rate [*Grant and Madsen*, 1979], thus increasing the transport rate.

The bottom shear stress coefficient (C_f) varied by an order of magnitude across the surf zone, with the values offshore and over the bar of the order of 10^{-3}, while the values in the trough were of the order of 10^{-2}. An attempt was made to find empirical relationships between C_f and measured physical parameters commonly used throughout the literature such as ($|\mathbf{u}_b|/V$) (ratio of near-bottom wave velocity magnitude from linear wave theory to mean current speed), the rms bottom roughness (r), and percent of wave breaking. Surprisingly, no statistically significant correlation was found between C_f and ($|\mathbf{u}_b|/V$).

C_f was found to be negatively correlated with percentage of wave breaking, with a linear correlation coefficient of −0.71, which is statistically significant at the 99% confidence level (Figure 12). This is contrary to the theoretical analyses of *Fredsoe and Deigaard* [1992] and *Church and Thornton* [1993].

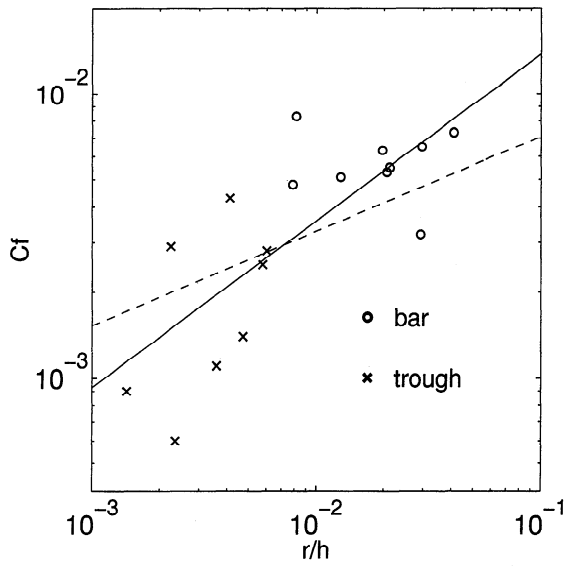

Figure 13. Bed shear stress coefficient (C_f) versus rms bottom roughness normalized by mean water depth (r/h). The dashed line is the Manning-Strickler equation (22), and the solid line is obtained by adjusting the coefficients of (22) by applying a linear regression least squares method to the data.

An effect associated with wave breaking in the surf zone is the generation of surface rollers that increases the mass transport within the surface layer, thus increasing the cross-shore return flow, or undertow, and, consequently, the average total velocity $(u^2 + v^2)^{1/2}v$. This effect reduces the C_f values calculated using (9) for increasing wave breaking. In addition, decreased C_f with increased wave breaking may be physically related to the planing off of wave ripples due to increased near-bottom velocities associated with wave breaking and consequent reduction of form drag, as well as to stratification caused by an intense vertical gradient of suspended sediment near the sea bed. This stratification can diminish the turbulent flow intensity in the bottom boundary layer, leading to reduced bottom stress [*Smith and McLean*, 1977a; *Taylor and Dyer*, 1977].

C_f would be expected to be related to bottom roughness due to enhanced form drag. The bottom roughness is examined by calculating wavenumber spectra of the bed. To calculate wavenumber spectra, the unevenly spaced data from the combined CRAB surveys and altimeter measurements are linearly interpolated to evenly spaced 2 cm increments of the cross-shore distance. The small-scale morphology in general shows large cross-shore variation; as a consequence, the condition of spatial homogeneity (stationarity) required for calculating averaged spectra is not met. Therefore continuous bottom roughness wavenumber spectra are calculated for 20 m cross-shore segments at increments of 1 m across the surf zone.

Lowest wave numbers are filtered by subtracting a third-order polynomial best fit curve from each 20 m section. A 10% cosine taper data window is applied to decrease spectral leakage. The spectra are summed over three wavelength bands (0.2–1.0, 1.0–3.33, and 3.33–20 m) plus the total band (0.2–20 m), resulting in 160, 28, 10, and 198 degrees of freedom for each band, respectively. The wavelength bands chosen are based on the examination of individual spectra. The spectra were generally broad, indicating that several ripple wavelengths coexisted as a result of newly formed ripples, combined possibly with residual ripples from the past to form a complex series of ripple patterns, plus the effects of alignment of ripples relative to the cross-shore measurement axis. The rms height of each band is calculated as the square root of the variance within each band. Note that variances sum, not rms heights, such that the rms height of the sum of the three bands is calculated from the square root of the sum of their variances. The rms bottom roughness (Figures 4b, 5b, and 6b) is dominated by longer wavelength features primarily associated with megaripples, with a small contribution from the superimposed shorter wavelength ripples O(1 m). The general trend being that bottom roughness was smoothest offshore and over the bar where wave ripples were planed off due to higher near-bottom velocities, with increased roughness within the trough associated with megaripples (for details, see *Thornton et al.* [1997]). The rms bottom roughness (r) is calculated from the total band (0.2–20 m) and thus includes contributions from both large- and small-scale morphology. Calculated values are listed in Table 1.

Roughness measurements were made in the cross-shore direction only. To relate C_f, calculated from the alongshore bed shear stress, to roughness, it is assumed that the bed forms are quasi-isotropic, which is not unreasonable for megaripples in the trough. However, this assumption is violated for long-crested wave ripples, such as those that occurred for the seventh run of October 11 when large wave ripples (observed in the side-scan sonar) were oriented parallel to the flow (alongshore direction), which results in overestimating the rms roughness associated with longshore currents at this cross-shore position. Altimeter data for October 12 is not available from 210 to 260 m because of the high false return levels induced by strong scattering of the acoustic pulses from air bubbles entrained by waves breaking over the bar. Therefore the CRAB survey data is used as the profile in this section, and hence the bottom is not as highly resolved in this area, compromising roughness estimates for the third, fourth, and fifth runs of October 12. Thus roughness data from these four runs, as well as data from the eighth run of October 11 (only two cms below the msl $- H_{\text{rms}}$ level) are disregarded.

If data from runs with logarithmic profile correlation coefficients <0.98 with resulting relative errors for $C_f > 50\%$ (Table 2) are also disregarded, only nine profiles could be used, making the ensemble too small to infer any statistically reliable relationship between C_f and bottom roughness. Therefore it was decided to use data from the remaining 17 profiles with the associated 95% confidence error estimates to examine the relationship between C_f and r. The bed shear stress coefficients are positively correlated with bottom roughness normalized by mean water depth (Figure 13), with a linear correlation coefficient of 0.63, which is statistically significant at the 99% confidence level.

The scatter of data observed in Figure 13 may be due to correlating the nonsynoptic velocity measurements with bottom roughness measured once in the morning, prior to the positioning of the sled for the first station. Wave forcing quantified by deep water wave height (H_0), period of peak wave frequency (T), and wave direction (θ) changed during the period of observation (Figure 1) because of both wind and tidal variations. Changes in wave forcing have a direct effect in the measured velocities and an indirect effect in bottom roughness due to modification of wave ripples associated with variations in wave height.

For steady currents (open channel flows), C_f depends only on bottom roughness when the bed is hydraulically rough, and

several empirical relationships (power laws) are available throughout the literature. One of the most widely used is the Manning-Strickler equation [*Sleath*, 1984, equation 5.86]

$$C_f = \frac{f_{DW}}{8} = 0.015\left(\frac{k_s}{h}\right)^{1/3} \tag{22}$$

where f_{DW} is the Darcy Weisbach friction coefficient and k_s is the bed roughness length scale or equivalent *Nikuradse* [1933] roughness of the bed.

In our definition of C_f (9), contributions from both steady and nonsteady velocity components were taken into account, whereas (22) applies to steady flow only. Nevertheless, during the period being analyzed the observed strong longshore current is not only the dominant term but is also well represented by a logarithmic profile (6). The flow can be classified as hydraulically rough as calculated Reynolds numbers ($k_s v_*/\mu$, in which μ = molecular kinematic viscosity coefficient) were >70 for all runs [*Schlichting*, 1979]. Thus, if measured rms bottom roughness is representative of the equivalent *Nikuradse* [1933] roughness of the bed ($k_s \approx r$), one might expect C_f to be related to (r/h) by a power law similar to (22). A plot of predicted C_f by the Manning-Strickler equation (22) is included in Figure 13, which shows an order of magnitude agreement between the data and predictions. These results suggest that the calculated rms bottom roughness (r) is representative of the bed roughness length scale or equivalent Nikuradse roughness of the bed (k_s).

The structure of the flow inside the wave boundary layer (WBL) is out of the scope of this paper as no measurements were made within this region. Outside the WBL, z_a is the proper length scale and not z_0 [*Grant and Madsen*, 1986]. Therefore the equivalent *Nikuradse* [1933] roughness of the bed (k_s) is replaced by an apparent bed roughness length scale (k_a). The flow is hydraulically rough during the period being analyzed, and thus k_a can be assumed to be given by ($k_a/30$) = z_a [*Nikuradse*, 1933]. Assuming that k_a is representative of the bed roughness length scale when waves and currents are present, an empirical relation (power law) between C_f and (k_a/h) is obtained by applying a linear regression least squares fit to the data to give

$$C_f = 0.011\left(\frac{k_a}{h}\right)^{1/2.75} \tag{23}$$

which is plotted in Figure 14. The rms error between measured and predicted C_f by (23) is 18%, which is within the 95% confidence band of the measurements. This is not surprising, as the coefficients of (23) were determined by fitting the data in a least squares sense. Nevertheless, the correlation between measured C_f and (k_a/h) is 0.80, which is statistically significant at the 99.5% confidence level, indicating that a power law relation between these parameters is not fortuitous.

An independent check of (23) is obtained by including the results from velocity profiles measured by *Grant et al.* [1984] on the northern California continental shelf in 90 m depth during the Coastal Ocean Dynamics Experiment (CODE) using four vertically stacked acoustic travel time current meters (benthic acoustic stress sensor (BASS)) mounted on tripods. A plot of measured C_f versus (k_a/h) for the CODE data (listed in Table 2 of their paper) is included in Figure 14. The agreement between C_f predicted by (23) and measured for the CODE data set is even better (rms error of 3.5%) than for the DUCK94 data set, which was used to determine the coefficients of (23).

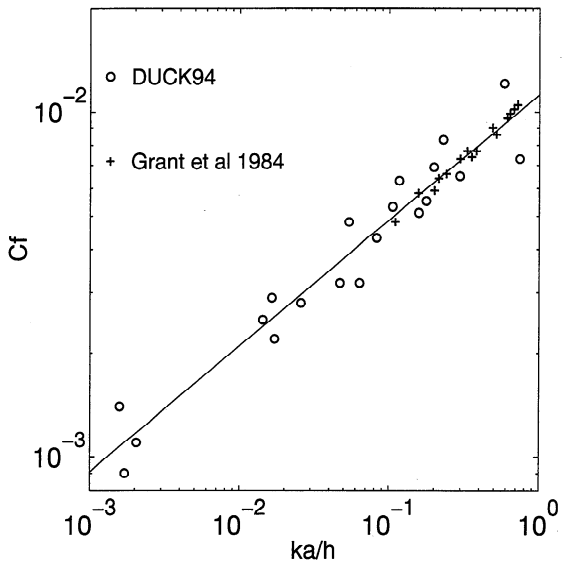

Figure 14. Bed shear stress coefficient (C_f) versus apparent bed roughness length scale normalized by mean water depth (k_a/h). The line represents predicted C_f by (23).

These results indicate that a single roughness length scale can be used to characterize combined flows over a movable bed, which is a basic assumption for all existing theoretical models. This assumption was shown to be valid for waves, currents, and combined flows over a fixed rippled bed by *Mathisen and Madsen* [1996].

Another reason for the scatter of data observed in Figure 13 arises from C_f values being calculated from the total bottom shear stress, which has stress contributions from skin friction related to sediment grains, wave-current nonlinear interactions within the bottom boundary layer, as well as form drag related to bed forms. *Smith and McLean* [1977b] linearly partitioned the total bed shear stress into skin friction and form drag and found good agreement with data from the Columbia River. *Nelson and Smith* [1989], *Wiberg and Nelson* [1992], and *Li* [1994] subsequently applied the linear partition concept to several flume experiments with good results. Extending this concept to the surf zone environment requires including an additional component due to nonlinear interactions between waves and currents within the bottom boundary layer to the total bed shear stress. Assuming that the linear stress partition is valid within the surf zone, the skin friction contribution can be removed from the total bottom stress, and a new bed shear stress coefficient C_f' is defined

$$C_f' = \frac{v_{*d}^2 + v_{*wc}^2}{(u^2 + v^2)^{1/2} v} \tag{24}$$

where v_{*d} and v_{*wc} are the form drag and wave-current interaction shear stress velocities. The relationship between C_f' and the total bed shear stress coefficient (C_f) can be determined from (9) and (24)

$$C_f' = \left[1 - \left(\frac{v_{*s}}{v_*}\right)^2\right] C_f \tag{25}$$

where v_{*s} is the skin friction related shear stress velocity.

As skin friction was not measured during the DUCK94 experiment, an attempt is made to isolate its contribution from

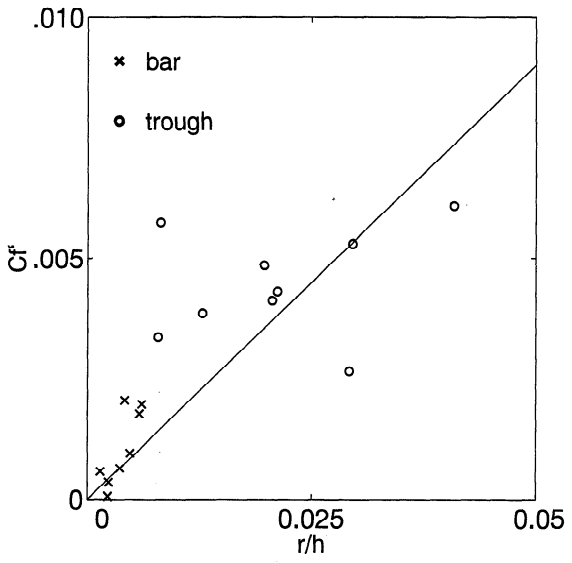

Figure 15. Bed shear stress coefficient without skin friction contribution (C_f') versus rms bottom roughness normalized by mean water depth (r/h). The line represents a linear regression with a regression coefficient of 0.76.

the total bottom shear stress by applying a stress partitioning model. The probabilistic approach used to quantify bottom roughness does not allow the adjustment of the two empirical coefficients C_D and a_1 necessary to apply the *Smith and McLean* [1977b] model. Therefore the empirical relationships obtained by *Li* [1994] by applying linear regression to the mean flow laboratory data of *Kapdasli and Dyer* [1986] and *Paola* [1983], as well as his own data obtained from mobile sand ripples, are used to estimate skin friction shear stress velocity from the total shear stress velocity obtained from the logarithmic profile

$$\frac{v_{*s}}{v_*} = 0.125\left(\frac{v_*}{R}\right) + 0.373 \qquad \frac{v_*}{R} < 2.3 \qquad (26)$$

$$\frac{v_{*s}}{v_*} = 0.107\left(\frac{v_*}{R}\right) + 0.266 \qquad \frac{v_*}{R} \geq 2.3 \qquad (27)$$

where R is ripple height, that is assumed here to be equal to the measured rms bottom roughness ($R = r$). For $(v_*/R) > 6.86$ the predicted v_{*s} by (27) is greater than the total measured shear stress velocity, and it is assumed that v_{*_s} is equal to 99% of the total shear stress whenever this occurred. Calculated values of v_{*_s} are listed in Table 1.

The recalculated bed shear stress coefficients C_f' by (25) show a higher linear correlation coefficient (0.76) with bottom roughness normalized by mean water depth (Figure 15). Theoretically, this is expected as the removal of the skin friction component from the total stress should enhance the form drag contribution and, consequently, increase the correlation between bed shear stress and bottom roughness. The improved correlation obtained by applying *Li*'s [1994] empirical relationships indicates that the linear stress partition concept introduced by *Smith and McLean* [1977b] can be extended to the surf zone environment, although a more detailed data set is necessary to validate these expressions.

5.4. Apparent Roughness Height

The change of mean current velocity profile due to the superposition of waves has been theoretically investigated over the last two decades, and several models have been presented [*Lundgren*, 1972; *Smith*, 1977; *Bakker and Van Doorn*, 1978; *Grant and Madsen*, 1979; *Fredsoe*, 1984; *Christoffersen and Jonsson*, 1985; *Myrhaug and Slaattelid*, 1989; *Sleath*, 1991]. A general approach common to all these works is splitting the mean velocity profile in an inner region close to the bed affected by turbulence produced in the wave boundary layer and an outer region above it, where the current is not directly affected by wave-current nonlinear interactions, so that the logarithmic profile (6) may be assumed to apply. The increased bed shear stress associated with wave-current interactions is modeled by replacing z_0 with z_a in (6).

The apparent roughness increase (z_a/z_0) is theoretically expected to depend on the relative current strength $(|\mathbf{u}_b|/V)$, the relative roughness (A_d/k_s) (ratio of the near-bottom wave semiorbital excursion from linear wave theory to equivalent *Nikuradse* [1933] roughness), and the angle between wave and current direction (ϕ). Several empirical relations for (z_a/z_0) based on these parameters have been obtained from laboratory experiments. Nevertheless, the applicability of these empirical relations to field data has not been verified, as previous field experiments, although containing reliable data on z_a, lack corresponding measurements of bottom roughness [*Grant et al.*, 1984; *Cacchione et al.*, 1987; *Lambrakos et al.*, 1988; *Slaattelid et al.*, 1990].

Three widely applied empirical relationships for (z_a/z_0) [*Coffey and Nielsen*, 1986; *Sleath*, 1991; *Van Rijn*, 1993] are tested using DUCK94 data, as measurements of both z_a and bottom roughness were made during this experiment. For hydraulically rough flows the physical roughness height can be estimated from $z_0 = (k_s/30)$ [*Nikuradse*, 1933], and once again the measured rms bottom roughness is used to represent the equivalent Nikuradse roughness of the bed ($k_s = r$).

No statistically significant correlation was found between observed (z_a/z_0) and the parameters $(|\mathbf{u}_b|/V)$, (A_d/k_s), and ϕ. Consequently, none of these empirical relations are able to accurately predict the apparent roughness increase for this data. These results, together with the scatter of available laboratory data on (z_a/z_0) [*Nielsen*, 1992, Figure 1.5.13] and difficulties associated with bottom roughness and velocity measurements within the WBL in the field, indicate that much remains to be done before a reliable empirical or theoretical relation for the apparent roughness height increase experienced by the mean current profile in the presence of waves is obtained.

6. Conclusions

The vertical structure of mean longshore currents on a barred beach is well described by a logarithmic profile for the three strong longshore current days examined. This hypothesis works better in the trough, where turbulent bottom boundary layer processes are more dominant, than over the bar, where breaking-wave-induced turbulence generated at the surface modifies the profile.

The modification of the mean longshore current profile within the surface layer in the presence of winds and waves is modeled by correcting the logarithmic profile predictions for measurements in an Eulerian frame with an undulating boundary for all ems located above the (msl $- H_{\text{rms}}$) level. The

addition of the alongshore component of the mass transport velocity corrects the underprediction of the modified logarithmic profile and improves the overall agreement with the data. Therefore it can be concluded that this simple model provides a first-order approximation that is sufficiently accurate to predict mean longshore currents within the surface layer.

The data indicate that wave breaking inside the surf zone decreases the bottom shear stress coefficient, which is contrary to the theoretical analyses of *Fredsoe and Deigaard* [1992] and *Church and Thornton* [1993]. This may be physically related to wave-breaking generated surface rollers that increase the cross-shore return flow (undertow) and, consequently, the average total velocity, decreasing C_f values calculated using (9), as well as to the planing off of wave ripples due to increased near-bottom velocities and consequent reduction of form drag and to stratification caused by an intense vertical gradient of suspended sediment near the sea bed.

The bed shear stress coefficient (C_f) varied by an order of magnitude across the surf zone (0.0006–0.012), with the values offshore and over the bar $O(10^{-3})$, while the values in the trough were $O(10^{-2})$. Thus longshore current and sediment transport models that assume C_f to be constant or mildly changing should be revised.

C_f was found to be directly proportional to bottom roughness, and hence bottom roughness is an important parameter to characterize the bottom boundary layer. The empirical relationships obtained by *Li* [1994] were used to remove the skin friction contribution from the total bottom shear stress. The improved correlation between bottom shear stress and bottom roughness obtained, although not conclusive to validate these simple expressions, indicates that the linear stress partition concept introduced by *Smith and McLean* [1977b] can be extended to the surf zone environment.

An empirical relation between C_f and apparent roughness length scale of the bed normalized by water depth (k_a/h) was obtained by applying a linear regression least squares fit to the DUCK94 data. Good agreement was also found between this relation and CODE data [*Grant et al.*, 1984], indicating that a single roughness length scale can be used to characterize combined wave-current flows over a movable bed.

Surprisingly, no statistically significant correlation was found between observed apparent roughness increase (z_a/z_0) and the parameters ($|\mathbf{u}_b|/V$), (A_d/k_s), and ϕ. Consequently, none of the three most used empirical relations for (z_a/z_0) [*Coffey and Nielsen*, 1986; *Sleath*, 1991; *Van Rijn*, 1993] were able to accurately predict the apparent roughness increase. These results indicate that despite improvements in our knowledge of turbulent boundary layers during the last two decades, we are still not able to estimate bottom roughness for field applications, which prevents the use of an empirical relation such as (23) or any other theoretical expression to predict the friction factor for combined waves and current flows.

Acknowledgments. This research was funded by the Office of Naval Research, Coastal Sciences Program, under contract N00114-95-AF-002. The authors wish to express their appreciation to all those who participated in the DUCK94 experiment, particularly the staff of the U.S. Army Field Research Facility under the direction of B. Birkemeier. In addition, special appreciation is expressed to R. Wyland, Naval Postgraduate School, for his role in the acquisition of wave and current data and to Jim Stockel and Mary Bristow, Naval Postgraduate School, for their help in processing data. We also would like to thank W. Dally, Florida Institute of Technology, for his thoughtful suggestions, which resulted in an improved paper.

References

Bagnold, R. A., An approach to the sediment transport problem from general physics, *U.S. Geol. Surv. Prof. Pap., 422-I*, 1–37, 1966.

Bailard, J. A., and D. L. Inman, An energetics bedload model for a plane sloping beach: Local transport, *J. Geophys. Res., 86*(C3), 2035–2043, 1981.

Bakker, W. T., and T. Van Doorn, Near bottom velocities in waves with a current, in *Proceedings of the 16th Coastal Engineering Conference*, pp. 1394–1413, Am. Soc. of Civ. Eng., New York, 1978.

Cacchione, D. A., W. D. Grant, D. E. Drake, and S. M. Glenn, Storm-dominated bottom boundary layer dynamics on the northern California continental shelf: Measurements and predictions, *J. Geophys. Res., 92*(C2), 1817–1827, 1987.

Christoffersen, J. B., and I. G. Jonsson, Bed friction and dissipation in a combined current and wave motion, *Ocean Eng., 12*(5), 387–423, 1985.

Church, J. C., and E. B. Thornton, Effects of breaking wave induced turbulence within a longshore current model, *Coastal Eng., 20*, 1–28, 1993.

Coffey, F. C., and P. Nielsen, The influence of waves on current profiles, in *Proceedings of the 20th Coastal Engineering Conference*, pp. 82–96, Am. Soc. of Civ. Eng., New York, 1986.

Deigaard, R., and J. Fredsoe, Shear stress distribution in dissipative water waves, *Coastal Eng., 13*, 357–378, 1989.

Dyer, K. R., Velocity profiles over a rippled bed and the threshold of movement of sand, *Estuarine Coastal Mar. Sci., 10*, 181–199, 1980.

Fredsoe, J., Turbulent boundary layer in wave-current motion, *J. Hydraul. Eng., 110*(8), 1103–1120, 1984.

Fredsoe, J., and R. Deigaard, *Mechanics of Coastal Sediment Transport*, 369 pp., World Sci., River Edge, N. J., 1992.

Gallagher, E. L., W. Boyd, S. Elgar, R. T. Guza, and B. Woodward, Performance of a sonar altimeter in the nearshore, *Mar. Geol., 133*, 241–248, 1996.

Garcez Faria, A. F., E. B. Thornton, and T. P. Stanton, A quasi-3D model of longshore currents, in *Proceedings of Coastal Dynamics '95*, pp. 389–400, Am. Soc. of Civ. Eng., New York, 1996.

Grant, W. D., and O. S. Madsen, Combined wave and current interaction with a rough bottom, *J. Geophys. Res., 84*(C4), 1797–1808, 1979.

Grant, W. D., and O. S. Madsen, The continental-shelf bottom boundary layer, *Ann. Rev. Fluid Mech., 18*, 265–305, 1986.

Grant, W. D., A. J. Williams III, and S. M. Glenn, Bottom stress estimates and their prediction on the northern California continental shelf during CODE-1: The importance of wave-current interaction, *J. Phys. Oceanogr., 14*, 506–527, 1984.

Gross, T. F., and A. R. M. Nowell, Mean flow and turbulence scaling in a tidal boundary layer, *Cont. Shelf Res., 2*, 109–126, 1983.

Gross, T. F., A. J. Williams III, and E. A. Terray, Bottom boundary layer spectral estimates in the presence of wave motions, *Cont. Shelf Res., 14*, 1239–1256, 1994.

Kapdasli, M. S., and K. R. Dyer, Threshold conditions for sand movement on a rippled bed, *Geophys. Mar. Lett., 10*, 45–49, 1986.

Lambrakos, K. F., D. Myrhaug, and O. H. Slaattelid, Seabed current boundary layers in wave-plus-current flow conditions, *J. Waterw. Port Coastal Ocean Div. Am. Soc. Civ. Eng., 114*(2), 161–174, 1988.

Li, M. Z., Direct skin friction measurements and stress partitioning over movable sand ripples, *J. Geophys. Res., 99*(C1), 791–799, 1994.

Lippmann, T. C., and R. A. Holman, Quantification of sand bar morphology: A video technique based on wave dissipation, *J. Geophys. Res., 94*(C1), 995–1001, 1989.

Lippmann, T. C., R. A. Holman, and K. K. Hathaway, Episodic, nonstationary behavior of a double bar system at Duck, North Carolina, U.S.A., 1986–1991, *J. Coastal Res., 15*, 49–75, 1993.

Lundgren, H., Turbulent currents in the presence of waves, in *Proceedings of the 13th Coastal Engineering Conference*, pp. 623–634, Am. Soc. of Civ. Eng., New York, 1972.

Mathisen, P. P., and O. S. Madsen, Waves and currents over a fixed rippled bed, 1, Bottom roughness experienced by waves in the presence and absence of currents, *J. Geophys. Res., 101*(C7), 16,533–16,542, 1996.

Myrhaug, D., and O. Slaattelid, Combined wave and current boundary layer model for fixed rough seabeds, *Ocean Eng., 16*(2), 119–142, 1989.

Nelson, J. M., and J. D. Smith, Mechanics of flow over ripples and dunes, *J. Geophys. Res., 94*(C6), 8146–8162, 1989.

Nielsen, P., *Coastal Bottom Boundary Layers and Sediment Transport*, 324 pp., World Sci., River Edge, N. J., 1992.

Nikuradse, J., Stromungsgesetze in glatten und rauhen rohren, *Work Rep. VD1*, 361 pp., 1933.

Paola, C., Flow and skin friction over natural rough beds, Sc.D. dissertation, Mass. Inst. of Technol./Woods Hole Oceanogr. Inst. Joint Program in Oceanogr., Woods Hole, 1983.

Philips, O. M., *The Dynamics of the Upper Ocean*, 336 pp., Cambridge Univ. Press, New York, 1977.

Rivero, F. J., and A. S. Arcilla, On the vertical distribution of $\langle \tilde{u}\tilde{w} \rangle$, *Coastal Eng.*, *25*, 137–152, 1995.

Schlichting, H., *Boundary Layer Theory*, 747 pp., McGraw-Hill, New York, 1979.

Simons, R. R., T. J. Grass, and M. Mansour-Tehrani, Bottom shear stresses in the boundary layers under waves and currents crossing at right angles, in *Proceedings of the 23rd Coastal Engineering Conference*, pp. 604–617, Am. Soc. of Civ. Eng., New York, 1992.

Slaattelid, O. H., D. Myrhaug, and K. F. Lambrakos, North Sea bottom steady boundary layer measurements, *J. Waterw. Port Coastal Ocean Div. Am. Soc. Civ. Eng.*, *116*(5), 614–633, 1990.

Sleath, J. F. A., *Sea Bed Mechanics*, 335 pp., John Wiley, New York, 1984.

Sleath, J. F. A., Velocities and bed friction in combined flows, in *Proceedings of the 22nd Coastal Engineering Conference*, pp. 450–463, Am. Soc. of Civ. Eng., New York, 1990.

Sleath, J. F. A., Velocities and shear stresses in wave-current flows, *J. Geophys. Res.*, *96*(C8), 15,237–15,244, 1991.

Smith, J. D., Modeling of sediment transport on continental shelves, in *Marine Modelling, The Sea*, vol. 6, edited by E. D. Goldberg et al., pp. 539–577, Wiley-Interscience, New York, 1977.

Smith, J. D., and S. R. McLean, Boundary layer adjustments to bottom topography and suspended sediment, in *Bottom Turbulence*, edited by J. C. J. Nihoul, pp. 123–151, Elsevier, New York, 1977a.

Smith, J. D., and S. R. McLean, Spatially averaged flow over a wavy surface, *J. Geophys. Res.*, *82*(C12), 1735–1746, 1977b.

Stive, M. J. F., and H. G. Wind, A study of radiation stress and set-up in the nearshore region, *Coastal Eng.*, *6*, 1–25, 1982.

Svendsen, I. A., and U. Putrevu, Nearshore mixing and dispersion, *Proc. R. Soc. London A*, *445*, 561–576, 1994.

Taylor, P. A., and K. R. Dyer, Theoretical models of flow near the bed and their implications for sediment transport, in *Marine Modelling, The Sea*, vol. 6, edited by E. D. Goldberg et al., pp. 579–601, Wiley-Interscience, New York, 1977.

Thornton, E. B., Variation of longshore currents across the surf zone, in *Proceedings of the 12th Coastal Engineering Conference*, pp. 291–308, Am. Soc. of Civ. Eng., New York, 1970.

Thornton, E. B., Energetics of breaking waves within the surf zone, *J. Geophys. Res.*, *84*(C8), 4931–4938, 1979.

Thornton, E. B., and R. T. Guza, Energy saturation and phase speeds measured on a natural beach, *J. Geophys. Res.*, *87*(C12), 9499–9508, 1982.

Thornton, E. B., J. L. Swayne, and J. R. Dingler, Small-scale morphology related to waves and currents across the surf zone, *Mar. Geol.*, in press, 1997.

Van Rijn, L. C., *Principles of Sediment Transport in Rivers, Estuaries and Coastal Areas*, 684 pp., Aqua Publ., Amsterdam, 1993.

Visser, P. J., Wave basin experiments on bottom friction due to current and waves, in *Proceedings of the 20th Coastal Engineering Conference*, pp. 807–821, Am. Soc. of Civ. Eng., New York, 1986.

Whitford, D. J., and E. B. Thornton, Comparison of wind and wave forcing of longshore currents, *Cont. Shelf Res.*, *13*, 1205–1218, 1993.

Wiberg, P. L., and J. M. Nelson, Unidirectional flow over asymmetric and symmetric ripples, *J. Geophys. Res.*, *97*(C8), 12,745–12,761, 1992.

A. F. Garcez Faria, Marinha, Diretoria de Hidrografia e Navegação, Rio de Janeiro 24048, Brazil. (e-mail: faria@oc.nps.navy.mil)

T. C. Lippmann, Scripps Institution of Oceanography, La Jolla, CA 92903. (e-mail: lippmann@coast.ucsd.edu)

C. V. Soares, Marinha, Instituto Hidrográfico, 1296 Lisboa Cedex, Portugal.

T. P. Stanton and E. B. Thornton, Department of Oceanography, Naval Postgraduate School, 833 Dyer Road, Monterey, CA 93943-5122. (e-mail: stanton@oc.nps.navy.mil; thornton@oc.nps.navy.mil)

(Received August 5, 1996; revised February 19, 1997; accepted May 21, 1997.)